Proceedings of ASME Turbo Expo 2011
GT2011
June 6-10, 2011, Vancouver, British Columbia, Canada

GT2011-46212

NUMERICAL CHARACTERIZATION OF AERODYNAMIC LOSSES OF JET ARRAYS FOR GAS TURBINE APPLICATIONS

Antonio Andreini, Riccardo Da Soghe
Energy Engineering Department "S.Stecco"
University of Florence
50139, via S.Marta 3, Florence, Italy
Tel: (+39)0554796618, Fax: (+39)0554796342
Email: riccardo.dasoghe@htc.de.unifi.it

ABSTRACT

Jet array is an arrangement typically used to cool several gas turbine parts. Some examples of such applications can be found in the impingement cooled region of gas turbine airfoils or in the turbine blade tip clearances control of large aero-engines. In order to correctly evaluate the impinging jet mass flow rate, the characterization of holes discharge coefficient is a compulsory activity. In this work an aerodynamic analysis of jet arrays for active clearance control was performed; the aim was the definition of a correlation for the discharge coefficient (C_d) of a generic hole of the array. The data were taken from a set of CFD RANS simulations, in which the behaviour of the cooling system was investigated over a wide range of fluid-dynamics conditions. More in detail, several different holes arrangements were investigated with the aim of evaluating the influence of the hole spacing on the discharge coefficient distribution. Tests were conducted by varying the jet Reynolds number in a wide range of effective engine operative conditions (Re=2000-12000,Pressure-Ratio=1.01-1.6). To point out the reliability of the CFD analysis, some comparisons with experimental data, measured at the "Department of Energy Engineering" of the University of Florence , were drawn. An in depth analysis of the numerical data set has underlined the opportunity of an efficient reduction through the mass velocity ratio of hole and feeding pipe: the dependence of the discharge coefficients from this parameter is roughly logarithmic.

NOMENCLATURE

A	Tube internal area	$[mm^2]$
Cd	Discharge coefficient	$[-]$
Cd^*	Scaled discharge coefficient	$[-]$
Cp	Pressure coefficient	$[-]$
d	Cooling hole diameter	$[mm]$
D	Tube internal diameter	$[mm]$
MV	Mass velocity ρv	$[kg/sm^2]$
MVR	Mass Velocity Ratio $(\rho v)_j/(\rho v)_c$	$[-]$
L	Tube length	$[mm]$
$\dot{m}$	Mass flow rate	$[kg/s]$
Ma	Mach number	$[-]$
P	Pressure	$[Pa]$
Re	Reynolds number	$[-]$
R	Gas constant	$[J/kgK]$
S	Pitch	$[mm]$
t	Wall thickness	$[mm]$
T	Temperature	$[C]$

Acronyms

Me	Million Elements
RMS	Root Mean Square
ACC	Active Clearance Control

Greeks

β	Global P ratio(P@manifold inlet /P@outlet)	$[-]$
β_L	Local pressure ratio	$[-]$
μ	Air viscosity	$[kg/ms]$
ρ	Air density	$[kg/m^3]$
γ	Heat capacity ratio	$[-]$

Subscripts

av	averaged value
c	main channel
d	discharge coinditions

i	i^{th} pressure taps
is	isentropic
j	jet impingement hole
s	static
t	total
x	streamwise direction

INTRODUCTION

Impingement with high velocity jets has become an established method for surface cooling or heating in a wide variety of processes and thermal control applications. The use of impingement jets for the cooling of modern aero-engine components is widespread, especially within the hot stationary parts. Since the cooling performance of impingement jets is very high, this method provides an efficient way to manage a component heat load when a sufficient pressure head and geometrical characteristics are available for its implementation. The cooling jets are usually arranged as arrays.

Aero-engine casing temperature control is an important aspect to reduce aerodynamic losses and specific fuel consumption due to blade tip clearance. Because of the significant variations of centrifugal and thermal loads occurring at different engine operating conditions, the tip clearance can be extremely variable; such dimensional variation may worst engine performance and reduce the components' life span [1]. To overcome those issues, the Active thermal Clearance Control (ACC), generally based on impingement cooling, has been successfully introduced in several applications as described in Halila et al. [2], Beck and Fasching [3] and more recently by Justak and Doux [1]. In such systems, impinging jets are directed on the external turbine casing by means of a series of circumferential feeding pipes with the final aim of keeping the clearance between blade tip and casing as constant as possible at different engine operating conditions.

In order to correctly evaluate the impinging jet mass flow rate, the characterization of the holes discharge coefficient is a fundamental activity.

The discharge coefficient (C_d) is defined as the ratio of the actual mass flow rate through the hole and the isentropic flow rate. It summarizes all the losses that limit the actual mass flow rate through a hole: entry pressure losses, holes interior losses due to friction and exit losses. In order to evaluate the C_d, the actual mass flow rate is measured while the ideal mass flow is calculated under certain hypothesis. Assuming an isentropic one-dimensional expansion through an orifice from coolant pipe (secondary flow) total pressure (P_t) to the main flow (primary flow) static pressure (P_d), the obtained expression is:

$$C_d = \frac{\dot{m}}{P_t \left(\frac{P_d}{P_t}\right)^{\frac{\gamma+1}{2\gamma}} \sqrt{\frac{2\gamma}{(\gamma-1)RT_t}\left(\left(\frac{P_t}{P_d}\right)^{\frac{\gamma-1}{\gamma}} - 1\right)} \frac{\pi}{4} d^2} \qquad (1)$$

Many parameters may influence the discharge coefficient [4]: geometrical, as hole shape, hole angle, space between holes, length to diameter ratio, etc., and fluid-dynamics, as pressure ratio across the hole, Reynolds and Mach number of the two cross-flows and inside the hole, etc. For this reason, several studies have been carried out on different geometries of holes subjected to a wide range of fluid-dynamics conditions; an extensive review can be found in Hay and Lampard [5].

More recently, Gritsch et al. [6] have investigated the behaviour of a single hole of large diameter (10 mm); they proposed a method for correlating the discharge coefficients, assuming that pressure losses inside the hole and those related to the hole entry and exit are independent. Internal losses are found to be dependent on the pressure ratio across the hole, while the entry and exit losses on the jet to cross-flow momentum ratio. With these hypotheses, Gritsch et al. [7] have studied the influence of the internal cross-flow on shaped holes, while Robwbury et al. [8] proposed a method to quantify the influence of external cross-flow on C_d. More recently, Schulz et al. [9] have performed several experiments, analyzing the behavior of C_d with varying internal and external cross-flow conditions and geometrical angles and using the jet-to-cross-flow momentum ratio to reduce data.

According to Thole et al. [10], the assumption that the source of pressure losses are independent seems not to be universally valid: the hole must be sufficiently long to permit the distortion of the inlet flow caused by the cross-flow decay before the outlet is reached. From the evidence of Hay et al. [11], L/d = 6 is certainly sufficient.

Quite interesting results on jet array impingement systems have been pointed out recently by Goodro and co-workers [12, 13, 14, 15, 16]. The authors revel that holes discharge coefficient is affected by both jet Reynolds and Mach number.

More recently Andreini and co-workers [17] performed a series of CFD RANS simulation on an aero-engine combustor liner. Final results of this work was the definition of a correlation for the discharge coefficient of the single effusion hole of the array expressed as a function of the ratio between the hole and the annulus Reynolds number, the inlet flow function and the velocity head ratio of the hole.

As seen above, many published works deal with C_d; most of them analyze, through experiments or numerical simulations, the behaviour of several hole geometries, investigating the different sources of loss but without giving indications on how to include their influence in an operating expression for the prediction of the C_d. Probably many of the correlations used by engine manufacturers are "in-house data" and are thus not freely available.

Therefore, despite the interest in the discharge coefficient, there are very few correlations available in the open literature for the single hole. From the literature overview presented above, it also appears a complete deficiency of general studies, and therefore of useful design correlations, concerning the effects on discharge coefficient due to the interaction among adjacent holes drilled in cylindrical feeding pipes. For these reasons, the authors decided to get a specific data set for cylindrical manifolds with impingement holes, through which to build a correlation for the C_d.

PURPOSE OF ANALYSIS

The scopes of the study are the analysis of the possible holes interactions and the definition of an expression to correlate the

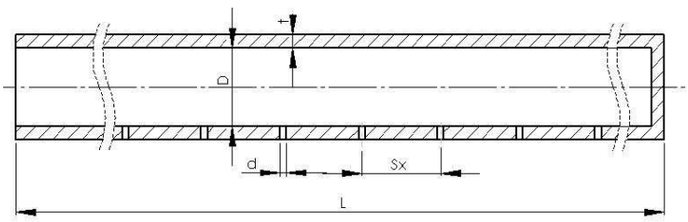

Figure 1. Tested geometries

holes discharge coefficients of the impingement holes array located on manifolds.

This work aims at a general characterization of the losses of the impingement cooling arrangements for ACC systems, allowing to isolate the effects of the main fluid-dynamics parameters. Such systems are usually composed of hole arrays drilled at 90^o with respect to the feeding pipe axis and the spent jets evolve in a quasi-quiescent environment.

Beside an investigation in a dedicated test rig (for a full description of the experimental apparatus, please refer to the work of Da Soghe et al. [18]), this study is carried out through an extensive numerical analysis. The study has been carried out, for a wide range of operating conditions, by varying the impingement system geometry. The analyzed geometries (figure 1) consist in cylindrical manifolds that are fed through one side while the other side is closed (i.e. the entire mass flow rate exits throughout the impingement holes). The tubes' length is $L = 400mm$ with a non dimensional tube thickness $t/d = 2$. In this work, several geometrical arrangements have been considered taking in to account the effects of manifold diameter, holes diameter, holes number and holes axial displacement. All the simulated geometries are reported in table 1.

Table 1. Impingement tubes arrangement

Geom. Label	D [mm]	d [mm]	S_x/d	oles number
A	12	1	1.5	134
B	12	1	6	34
C	12	1	12	12
D	6	1	1.5	34
E	6	1	3	34
F	6	1	6	34
G	12	2	3	34
H	12	1	1.5	34
I	12	1	3	34

The rationale for these configurations will be clear through the text. The numerical domain, shown in figure 2, consists in the impinging system that discharges in a plenum whose overall dimensions are $500X500X500[mm]$. As the impingement holes discharge in a quiescent environment, the effect of the external flow on the holes C_d is not evaluated in this work.

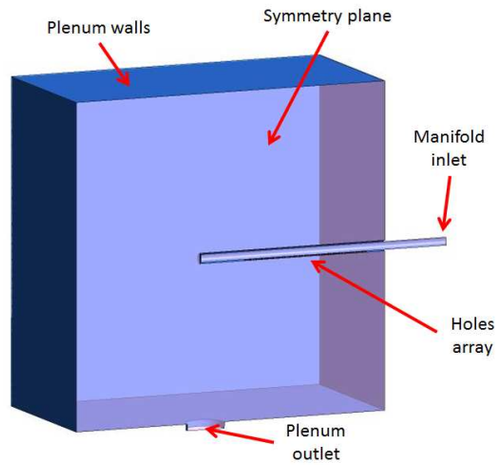

Figure 2. Numerical domain

The operating conditions of the geometries are reported in table 2.

Table 2. Operating conditions

Geom. Label	β
A	1.01, 1.04, 1.08, 1.12, 1,22, 1.3
B	1.09, 1.18, 1.32, 1.6
C	1.08, 1.2, 1.3, 1.54
D	1.1, 1.65
E	1.1, 1.65
F	1,1, 1.65
G	1.42
H	1.09, 1.6
I	1.09, 1.6

To calculate the C_d, the upstream fluid-dynamic quantities were calculated above the inlet of each hole, on the centerline of the manifold, while the discharge static pressure was evaluated within the plenum. Both the isentropic mass flow rate and the local pressure ratio were evaluated using static quantities.

From the post-processing of the CFD results, values of discharge coefficient for each impingement hole were extracted for each simulation, allowing to get a data set of more than 1300 C_d evaluations.

CFD COMPUTATIONS

CFD steady state calculations have been performed with the commercial 3D Navier-Stokes solver Ansys®CFX v.12.0.

A symmetry condition has been imposed at the facility symmetry plane while no-slip and adiabatic conditions have been applied on solid surfaces. The pressure boundary condition has been imposed at the outlet while mass flow rates were fixed at the inlet.

Compressibility effects have been taken into account and a 2^{nd} order Upwind advection schemes have been used. The fluid has been modelled as ideal gas and the properties of specific heat capacity, thermal conductivity and viscosity have been assumed as constants.

Energy equation has been solved in terms of total temperature and viscous heating effects have been accounted for.

The k-ω-SST turbulence model, in its formulation made available by the CFD solver, has been used in conjunction with a high Reynolds approach.

The convergence of solutions has been assessed by monitoring mass flow through the outlet and residuals. Furthermore the runs have been stopped when the pressure level and other physical quantities on different locations, reached a steady state.

The mesh generation tool Ansys®ICEM-CFD has been used to generate a tetrahedral cell mesh. A number of grid sensitivity

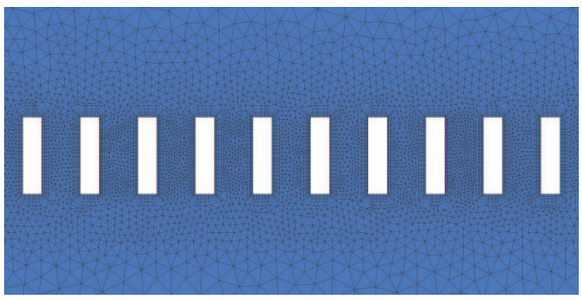

Figure 3. CFD mesh: Geometry A standard grid

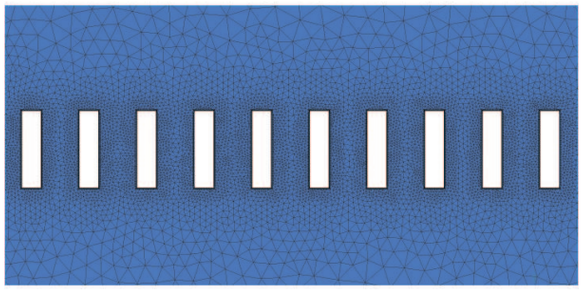

Figure 4. CFD mesh: Geometry A refined grid

tests have been carried out in order to ensure mesh independent solutions. Some findings of this analysis are shown in figures 5 and 6 where the results obtained by the use of the standard mesh selected for the geometry A (3 Me and $y^+ > 15$, figure 3), have been compared with the predictions evaluated using a more refined mesh (8 Me and $y^+ > 5$, figure 4). The refined mesh has been generated reducing the grid y^+ values within the impingement holes and refining the grid size just close to the holes. Far away from the holes, the grids are the same. Bearing in mind that the original mesh counts 3 million elements and the refined one 8 million elements, this means that the elements for each hole are, in the refined mesh, more than double of those related to the standard mesh.

As shown by the figures, the two meshes provide a rather similar distribution of the mass flow rates across the 134 holes and the same static pressure distribution within the manifold. Thus, it can be assumed that mesh independent solutions are achieved using the standard grid. Similar conclusions have been pointed out for the other operating conditions and other geometries analyzed in this work.

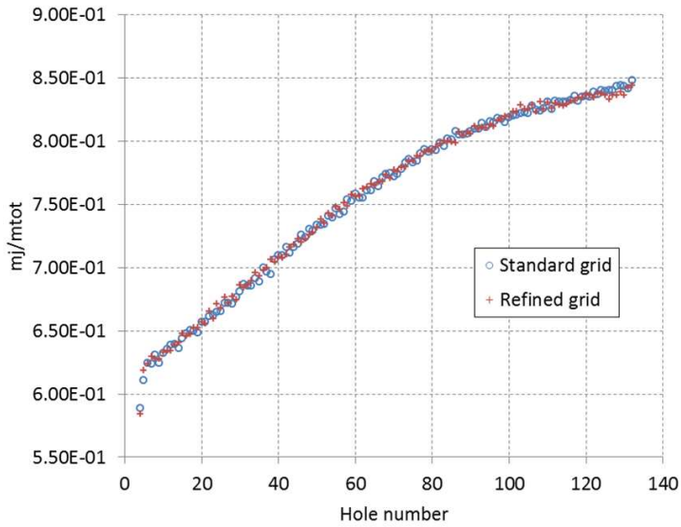

Figure 5. CFD mesh sensitivity: Geometry A mass flow rate split in case of $\beta = 1.12$

A preliminary validation of the numerical setup was carried out by the authors in a previous work where the experimental analysis performed by Schulz et al. [9] was successfully replicated using a similar CFD methodology (Andreini et al. [17]).

In order to further assess the CFD predictions reliability, a comparison between the pressure profiles evaluated within the supply pipe and the related dedicated experimental data has been drawn. The experimental data have been established through an extensive experimental campaign performed on a dedicated test rig developed and operated at the ”Department of Energy Engineering” of the University of Florence. The experiments have considered the geometries labelled A, B and C and have provided reliable evaluation of the pressure profiles within the manifolds. Within the test bed, the pressure levels have been measured through five pressure taps along the manifold that result in

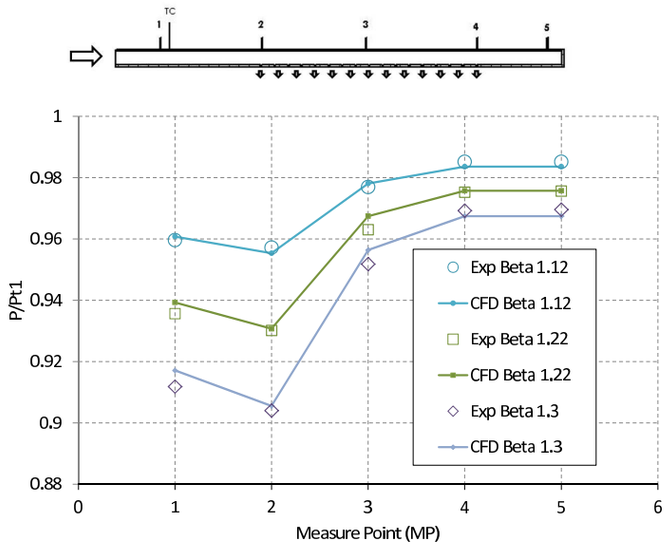

Figure 6. Comparison between CFD and experimental results in terms of manifold centerline pressure distribution

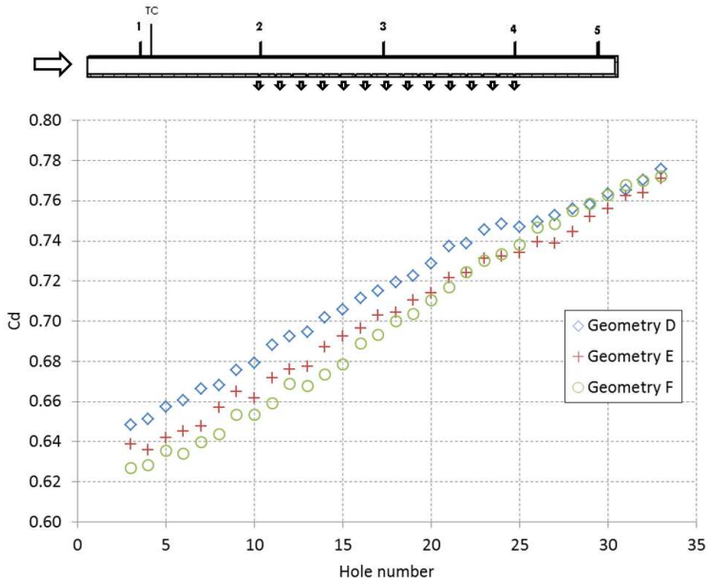

Figure 7. Discharge coefficient distribution: Geometry D, E, F β=1.1

five measure points (MP) (see the upper part of figure 6). For further details regarding the experimental analysis please refer to Da Soghe et al. [18].

Figure 6 reports the pressure profiles evaluated for the geometry A. In a wide range of operating conditions (i.e. in a wide range of overall β ratio), the CFD predictions are in fairly good agreement with the experimental data. Similar conclusions have been drawn for other geometries analysed in this work. Considering that the static pressure profile is closely related to the mass flow rate distribution across the impingement holes, the CFD can be considered a reliable tool for the system discharge behaviour prediction and it can be safely used to extend experimental test matrix.

RESULTS

Effects of S_x/d parameter on the holes C_d

The effects of the holes spacing on the discharge coefficient have been analyzed by focusing on geometries labelled D, E and F. For these geometries, trends of C_d plotted versus the increasing hole number are presented in figure 7. The first and the last holes are not considered because their behaviour is affected by the border effects and differs significantly from the others.

The impact of the holes spacing is appreciable for the first manifold holes and becomes less appreciable when approaching the manifold end. The geometry with the higher holes pitch shows lower values of the local discharge coefficient. This last evidence could be motivated by observing that the increase of the S_x/d parameters leads to a cross-flow much more aligned to the manifold axis. The increase of the flow angle at the hole inlet leads to stronger inlet losses and then lower values of discharge coefficient are appreciated. These effects are purely related to the jet to cross flow momentum ratio and then, as confirmed by figure 7, they become negligible when approaching the manifolds end. The above described phenomenon is however quantitatively comprised in the range of 4% concerning the CFD evaluated discharge coefficient. As the last evidence is also true for the other operating conditions simulated here, the S_x/d parameter will not account for the definition of impingement hole C_d correlation.

Data reduction

Trends of C_d plotted versus the increasing hole number are presented in figure 8 for the geometry labelled A. The plot shows

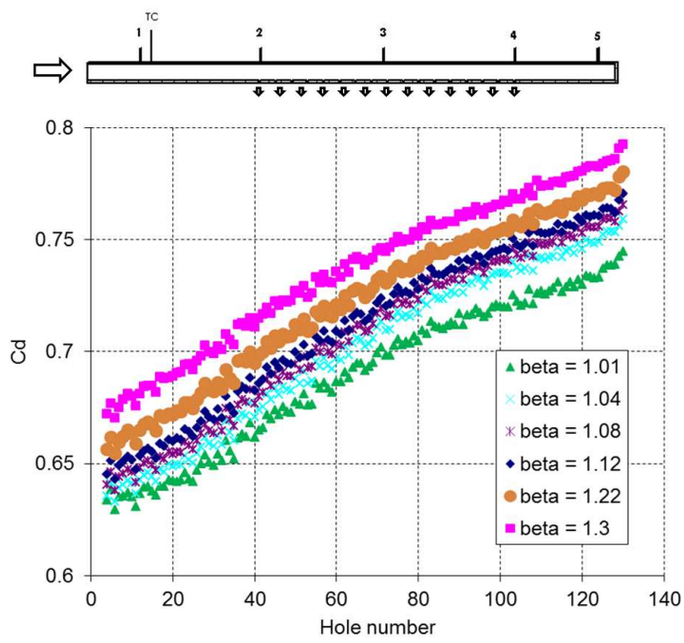

Figure 8. Discharge coefficient distribution: Geometry A

how the C_d increases quite linearly towards the end of the manifold, indicating a direct relation with the coolant mass flow left in the annulus. All the simulations have the same rate of in-

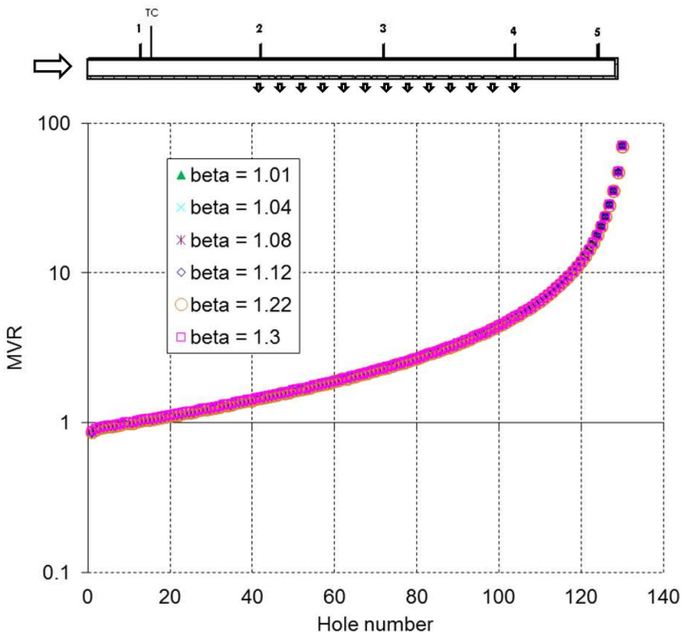

Figure 9. MVR parameter distribution: Geometry A

crease, and from figure 9 it emerges that the mass velocity ratio MVR (and, as a consequence, the mass flow rate split across the manifold) is not related to the fluid-dynamic operating conditions but is only related to the geometry of the manifold. Figure 10 shows the C_d distribution over the MVR parameter for all cases of group A. It emerges from the figure that the discharge coefficient is quite sensible to the mass flow velocity ratio for MVR values below 5 circa, while it is quite independent from this parameter for MVR high values. This means that the influence of the internal cross flow on the C_d is only relevant for low values of MVR. Furthermore, when the influence of the internal cross flow is relevant, the dependence of the discharge coefficient on the MVR is roughly logarithmic.

The reduction of the discharge coefficient at low MVR region could be directly related to the increase of the flow angle (measured from the holes axis) at the hole inlet section with the decrease of the MVR parameter. The increase of the flow angle leads to a more severe separation zone. As the hole has a circular shape it is expected that the vena-contracta area changes in a steeper way than a simple linear function of the separated flow region extension (i.e. with the flow angle at the inlet of the impingement hole). This can explain why the Cd shows the logarithmic like behavior here reported. It is also expected that different hole shape may leads to different Cd behavior at low MVR region.

This effect is also confirmed by figure 11 which shows the discharge coefficients evaluated for the geometries B, H, I. For these geometries, the high values of the MVR parameter lead to

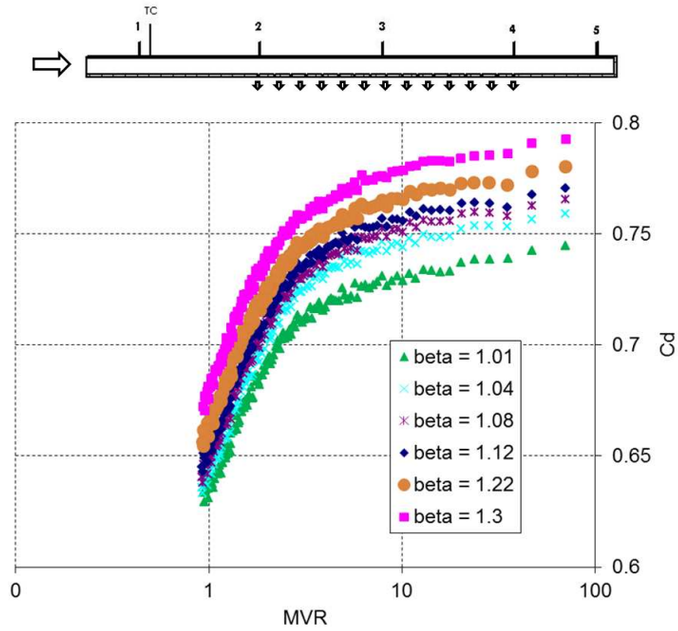

Figure 10. Discharge coefficient over MVR parameter distribution: Geometry A

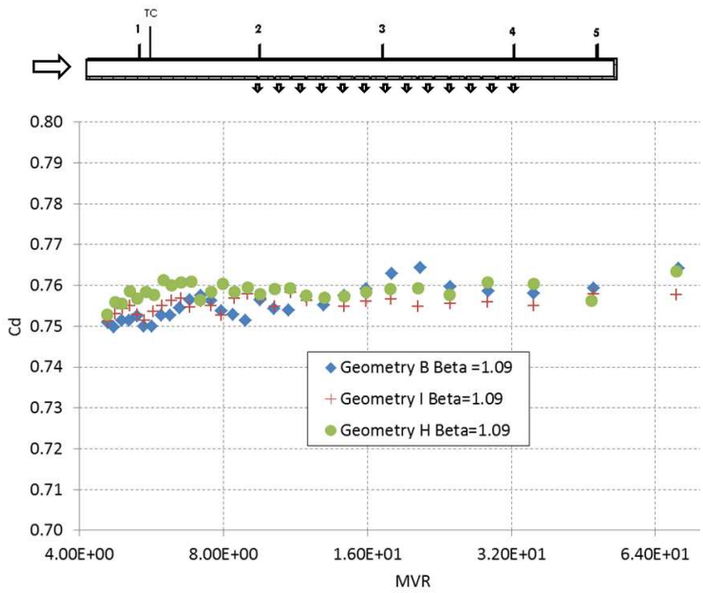

Figure 11. Discharge coefficient over MVR parameter distribution: Geometry B, H, I

flat C_d profiles.

In order to lump the effect of the operating condition in the C_d, the calculated discharge coefficients were scaled with the hole local β_L ratio elevated to a suitable constant:

$$C_d^* = \frac{C_d}{\beta_L^\alpha} \tag{2}$$

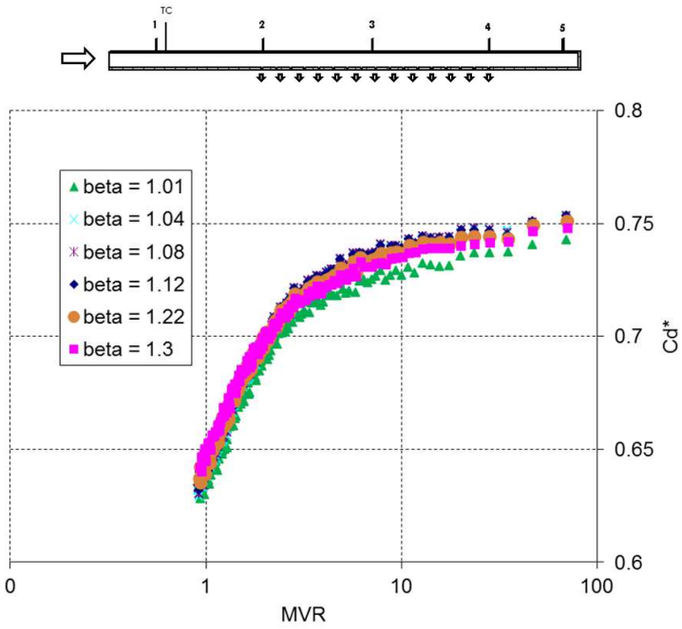

Figure 12. C_d^* over MVR parameter distribution: Case A, $\alpha = 0.19$

Figure 12 shows the scaled discharge coefficient C_d^* as a function of the MVR parameter evaluated for geometry A. The figure reveals that the obtained numerical data collapse quite well and so it is assumed that C_d can be expressed as a function of the local pressure ratio and the local MVR:

$$C_d = f(\beta_L, MVR) \tag{3}$$

Figure 13 points out that the reduction procedure fits with the whole CFD data set (i.e. all geometries and related operating conditions considered in this work). The generic hole β_L ratio allows a local correction of the value predicted using the MVR parameter, increasing the global accuracy of the correlation. In order to separate the effects of the cross flow on the C_d, the discharge coefficient of the single hole will be expressed as a product of two terms:

$$C_d = C_{d\_noCrFlow} \cdot C_{d\_IntCrFlow} \tag{4}$$

where

$$C_{d\_noCrFlow} = a \cdot \beta_L^{\alpha} \tag{5}$$

and

$$C_{d\_IntCrFlow} = (1 + b \cdot c^{d \cdot MVR^{\gamma}}) \tag{6}$$

The six coefficients of the correlation were calculated minimizing the RMS through the interpolation, with the expression 6, of the 1300 values of discharge coefficients extracted from the CFD: a mean relative error of 0.8% and a maximum of 3.5% was computed, with a standard deviation of 0.6% (i.e. 95% of the C_d predicted when using the correlation leads to an error lower than 2% with respect to the CFD data set). Table 3 reports the suggested correlation coefficients.

Table 3. Correlation coefficients

Coefficient	Value
a	0.745
b	1262
c	3.1
d	-8
α	0.19
γ	0.1124

In figure 14, the values of the C_d^* values predicted through the correlation are compared with those predicted by the CFD for all geometries and operating conditions considered in this paper. The figure shows that a quite good agreement between CFD and correlation is achieved for all geometries and operating conditions.

Suggested design practices

Let's now discuss on how the derived correlation can be used to define an useful design practice to design a manifold fed impinging system.

As pointed out above, the mass velocity ratio is not related to the manifold operating conditions but it is related to its geometry. Figure 15 shows the MVR parameter evaluated for several geometries and operating conditions. The geometries are characterized by different impingement holes diameter, holes spacing and manifold diameter while the ratio of the manifold inlet area and total holes exit area is kept constant. As shown in figure 15, the MVR distribution obtained for the mentioned geometries is the same and therefore it can be definitively assumed that the mass flow rate split across the impingement system is only related to the ratio of the manifold inlet area and total holes exit area. Figures 10, 11 and 14 reveal that, for a each operating condition (i.e. for each β ratio) the discharge coefficient is roughly constant for MVR higher than 5.

As the MVR is a function of the ratio between the manifold inlet area and total holes exit area, it is possible to design the impingement system in order to assure that the mass flow rate through each hole is roughly the same. Indeed, assuming that the manifold inlet mass flow rate is equally distributed among the impingement holes, it follows that:

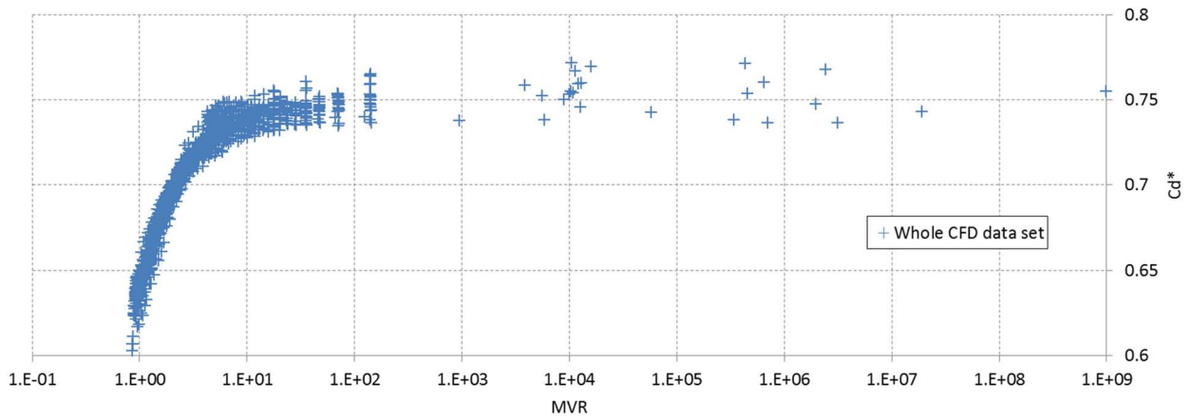

Figure 13. C_d^* over MVR parameter distribution: Whole CFD data set (i.e. all geometries and related operating conditions

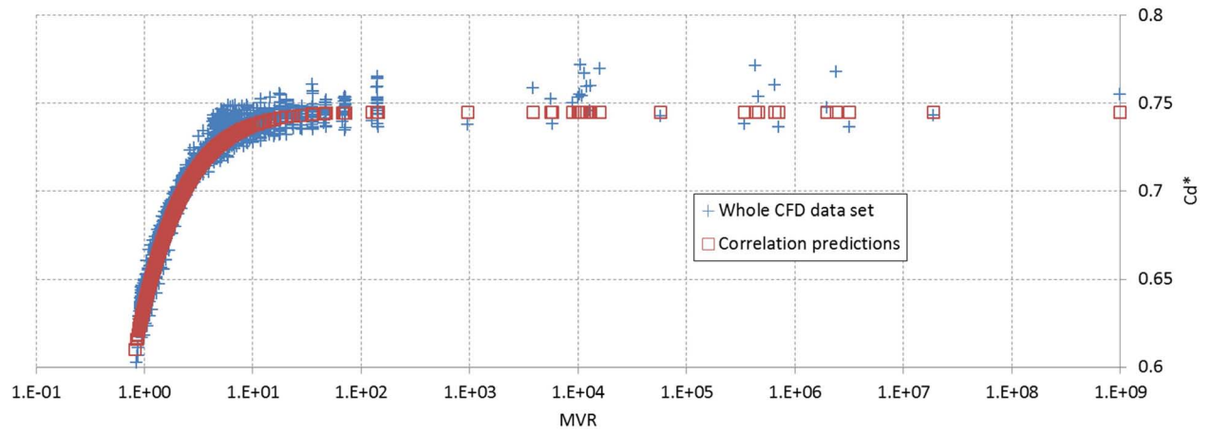

Figure 14. C_d^* over MVR parameter distribution: Comparison among correlation prediction and whole CFD data set (i.e. all geometries and related operating conditions

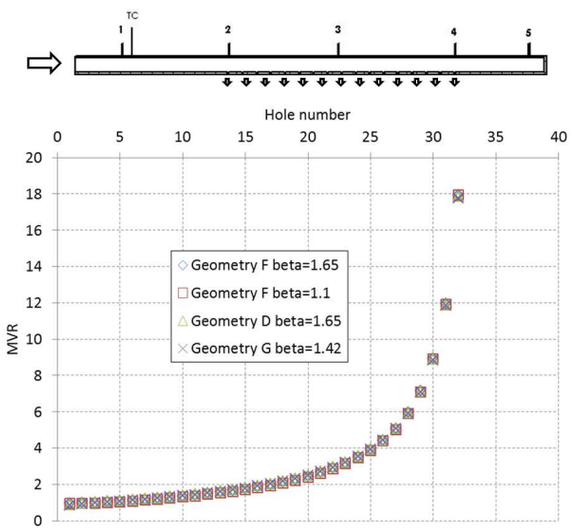

Figure 15. MVR parameter distribution: Several geometries and boundary conditions

$$A_c \cdot (\rho \cdot v)_c = n_{holes} \cdot A_j \cdot (\rho \cdot v)_j \tag{7}$$

$$MVR = \frac{A_c}{n_{holes} \cdot A_j} \tag{8}$$

The relations above are satisfied when the C_d is constant across the impingement system i.e. for MVR higher than 5 approx. So it can be assumed that the condition:

$$\frac{A_c}{n_{holes} \cdot A_j} > 5 \tag{9}$$

define a design rule for manifolds with equally distributed impinging mass flow rate jets.

CONCLUSIONS AND PERSPECTIVES FOR FUTURE WORK

A three dimensional CFD analysis was performed in order to investigate the aerodynamic losses of impingement holes array

located on manifolds; the investigation was carried out with the use of a test matrix of numerical simulations, which allowed to analyze several geometries typically implemented in ACC systems, over a wide range of fluid-dynamics conditions.

The analysis takes into account several geometrical aspects i.e. the number of impinging holes, their diameter, the holes spacing and the manifold diameter.

The CFD results were preliminary validated by the data obtained through a dedicated experimental campaign carried out on a test rig at the "Department of Energy Engineering" of the University of Florence.

The study led to the development of an empirical correlation for the prediction of the discharge coefficient: it expresses the C_d of each impingement hole as a function of the ratio between the hole and the manifold mass velocity and the local value of the β_L ratio.

The correlation was deduced from the analysis of the discharge coefficients extracted from the numerical simulations; it reproduces the trend of the C_d with an average relative error of 0.8% and a maximum error of 3.5% over the whole range of fluid-dynamics and geometrical conditions. Finally, the study has revealed that the effects of the holes axial displacement has a weak effect on the discharge coefficient so that this parameter has not been taken into account for the C_d correlation.

Although the correlation has been developed focusing on ACC systems, it could be useful for other gas turbine applications based on impingement cooling, i.e. airfoil leading edge and trailing edge impingement cooling (Han et al. [19], Halila et al. [2]), endwall cooling (Halila et al. [2]) and so on. In this way, the authors recognize that the impact on the discharge coefficient of both the external flow and t/d ratio should be accounted for to provide a correlation for more general applications. This will be done by the authors in the near future defining new multiplying correction terms ($C_{d\_ExtCrFlow}$ and $C_{d\_t/d}$) function of the external cross flow and t/d ratio.

ACKNOWLEDGMENT

The authors wish to express their gratitude to F. Maiuolo and L. Tarchi for providing the experimental data and AVIO Group for financial support. The authors are also grateful to Prof. Bruno Facchini for his useful suggestions.

REFERENCES

[1] Justak, J. F., and Doux, C., 2009. "Self-acting clearance control for turbine blade outer air seals". *ASME, Turbo Expo*, **GT2009-59683**.

[2] Halila, E., Lenahan, D., and Thomas, T., 1982. *High Pressure Turbine Test Hardware*. NASA CR-167955.

[3] Beck, B., and Fasching, W., 1982. *CF6 Jet Engine Performance Improvement - Low Pressure Turbine Active Clearance Control*. NASA CR-165557.

[4] Lefebvre, A., 1998. *Gas Turbine Combustion*. Taylor & Francis.

[5] Hay, N., and Lampard, D., 1998. "Discharge coefficient of turbine cooling holes: a review". *ASME, Journal of Turbomachinery,* **Vol. 120, pp. 314-319**.

[6] Gritsch, M., Schulz, A., and Wittig, S., 1998. "Method of correlating discharge coefficient of film-cooling holes". *AIAA Journal,* **Vol. 36/3, pp. 976-980**.

[7] et al., M. G., 1999. "Effect of internal coolant crossflow orientation on the discharge coefficient of shaped film cooling holes". *ASME, Turbo Expo,* **99-GT-40**.

[8] Rowbury, D., Oldfield, M., and Lock, G., 2001. "A method for correlating the influence of external crossflow on the discharge coefficients of film cooling holes". *ASME, Journal of Turbomachinery,* **Vol. 123, pp. 258-265**.

[9] Schulz, A., Gritsch, M., and Wittig, S., 2001. "Effect of crossflows on the discharge coefficient of film cooling holes with varying angles of inclination". *ASME, Turbo Expo,* **2001-GT-0134**.

[10] Thole, K., and al., 1997. "Effect of a cross-flow at the entrance to a film-cooling hole". *Journal of Fluids Engineering,* **Vol. 119/3, pp. 533-541**.

[11] Hay, N., Lampard, D., and Khaldi, A., 1994. "The coefficient of discharge of 30 inclined film cooling holes with rounded entries or exits". *ASME, Turbo Expo,* **94-GT-180**.

[12] Goodro, M., Park, J., Ligrani, P. M., Fox, M., and Moon, H.-K., 2007. "Effects of mach number and reynolds number on jet array impingement heat transfer". *International Journal of Heat and Mass Transfer,* **Vol. 50, No. 1, pp. 367-380**.

[13] Park, J., Goodro, M., Ligrani, P. M., Fox, M., and Moon, H.-K., 2007. "Separate effects of mach number and reynolds number on jet array impingement heat transfer". *ASME, Journal of Turbomachinery,* **Vol. 129, No. 2, pp. 269-280**.

[14] Goodro, M., Park, J., Ligrani, P. M., Fox, M., and Moon, H.-K., 2008. "Effect of hole spacing on spatially-resolved jet array impingement heat transfer". *International Journal of Heat and Mass Transfer,* **Vol. 51, Nos. 25-26, pp. 6243-6253**.

[15] Goodro, M., Park, J., Ligrani, P. M., Fox, M., and Moon, H.-K., 2009. "Effect of temperature ratio on jet array impingement heat transfer". *ASME, Journal of Heat Transfer,* **Vol. 131, No. 1, Pages 012201-1 to 12201-10**.

[16] Goodro, M., Park, J., Ligrani, P. M., Fox, M., and Moon, H.-K., 2010. "Mach number, reynolds number, jet spacing variations: Full array of impinging jets". *AIAA Journal of Thermophysics and Heat Transfer,* **Vol. 24, No. 1, pp. 133-144**.

[17] Andreini, A., Bonini, A., Caciolli, G., Facchini, B., and Taddei, S., 2010. "Numerical study of aerodynamic losses of effusion cooling holes in aero-engine combustor liners". *ASME, Turbo Expo,* **GT2010-22942**.

[18] DaSoghe, R., Maiuolo., F., Tarchi, L., Micio, M., and Facchini, B., 2011. "Discharge coefficient characterization of jet array impingement holes for an active clearance control system". *ETC,* **ETC2011-252**.

[19] Han, J. C., Dutta, S., and Ekkad, S., 2000. *Gas Turbine Heat Transfer and Cooling Technology*. Taylor & Francis.